P H Y S I C A L   R E V I E W   L E T T E R S

Mechanism for Room-Temperature Single-Atom Lateral Manipulations on Semiconductors using Dynamic Force Microscopy

Yoshiaki Sugimoto,[1] Pavel Jelinek,[2] Pablo Pou,[3] Masayuki Abe,[1,4] Seizo Morita,[1] Ruben Perez,[3] and Oscar Custance[1]

[1]*Graduate School of Engineering, Osaka University, 2-1 Yamada-Oka, 565-0871 Suita, Osaka, Japan*
[2]*Institute of Physics, Academy of Sciences of the Czech Republic, Cukrovarnicka 10, 1862 53, Prague, Czech Republic*
[3]*Departamento de Física Teórica de la Materia Condensada, Universidad Autónoma de Madrid, 28049 Madrid, Spain*
[4]*PRESTO, Japan Science and Technology Agency, Saitama 332-0012, Japan*

Vacancy-mediated lateral manipulations of intrinsic adatoms of the Si(111)-(7 × 7) surface at room temperature are reported. The topographic signal during the manipulation combined with force spectroscopy measurements reveals that these manipulations can be ascribed to the so-called pulling mode, and that the Si adatoms were manipulated in the attractive tip-surface interaction regime at the relatively low short-range force value associated to the manipulation set point. First-principles calculations reveal that the presence of the tip induces structural relaxations that weaken the adatom surface bonds and manifests in a considerable local reduction of the natural diffusion barriers to adjacent adsorption positions. Close to the short-range forces measured in the experiments, these barriers are lowered near the limit that enables a thermally activated hopping at room temperature.

PACS numbers: 81.16.Ta, 07.05.Tp, 68.37.Ps

Since the first demonstration of atom-by-atom assembly [1], well-controlled lateral manipulations using scanning tunneling microscopy (STM) have provided a fascinating tool for stunning realizations in nanoscale science [2–5]. In most of those experiments, atoms and molecules were individually dragged over the surface upon an enough tip vertical proximity [6]. To do so, the thermal and mechanical stability provided by a cryogenic environment was a requirement. Recently, a new exciting panorama has been opened with the ability of dynamic force microscopy (DFM) to atom-by-atom manipulations with sophisticated nanostructuring at semiconductor surfaces under room-temperature (RT) conditions [7].

To shed some light on the detailed mechanism behind these novel RT manipulations on semiconductors using DFM, in this Letter, we clarify the mechanism for the lateral manipulation of intrinsic adatoms of the Si(111)-(7 × 7) surface in the presence of a single atomic vacancy at RT. By combining experiments and first-principles calculations, we show that, for the measured attractive short-range (SR) forces associated with the manipulation set point, the presence of the semiconductor tip lowers, very locally, the energy barriers for the adatoms' natural diffusion near the limit that enables the thermally activated hopping between adjacent adsorption sites.

The experiments were performed using a home-built atomic force microscope (AFM) in ultrahigh vacuum environment operated [8] under the frequency modulation detection method [9], keeping the cantilever oscillation amplitude constant and the electrostatic interaction minimized. Details about the RT force spectroscopy acquisition and analysis protocols can be found in Refs. [10,11]. The same tip apex was used to perform the lateral manipulations and the subsequent spectroscopic measurements as

neither spontaneous image contrast changes nor instabilities in the spectroscopic curves were detected. The Si tip and the sample preparation is described elsewhere [12].

Figure 1 shows a selection of images from a series of sequential manipulations of adatoms within a faulted half-unit cell [13] in the presence of an atomic vacancy, which is used as an open space to enhance the adatoms' mobility at RT. These atomic vacancies can be created [12,14] or occasionally found. The adatoms adjacent to a vacancy can be individually manipulated along a path parallel to the dimer rows [Figs. 1(a)–1(f)], and across the half-unit cell [Figs. 1(f)–1(h)], splitting the vacancy in two parts at the intermediate adsorption position shown in Fig. 1(g). These unusual adsorption positions (*M* sites), in which the adatom sits in a T_4 configuration bonded to one of the three original surface rest atoms [Figs. 1(g) and 1(i)], are as stable as the usual adsorption sites, being possible to image them during hours at weak enough tip-surface interaction forces.

These manipulations have been performed using a similar protocol to the one reported in Ref. [7]. The fast scan direction was aligned parallel to the dimer-row, scanning from the adatom to be manipulated towards the vacancy lifting the tip up ~1 Å on the way back [Fig. 1(d)]. The slow scan was stopped near the topmost part of the targeted adatom, and subsequent scans over this line were performed at a higher tip-surface interaction (Δf_M) until the adatom was manipulated. Finally, the initial imaging set point (Δf_I) was restored. An appropriate selection of the fast scan length makes it possible to relocate an adatom on these unusual *M* positions, as in Fig. 1(g).

Figure 2(c) shows the topography during the manipulation process between the images in Figs. 1(d) and 1(e). The adatom manipulation takes place in the stripe enclosed by
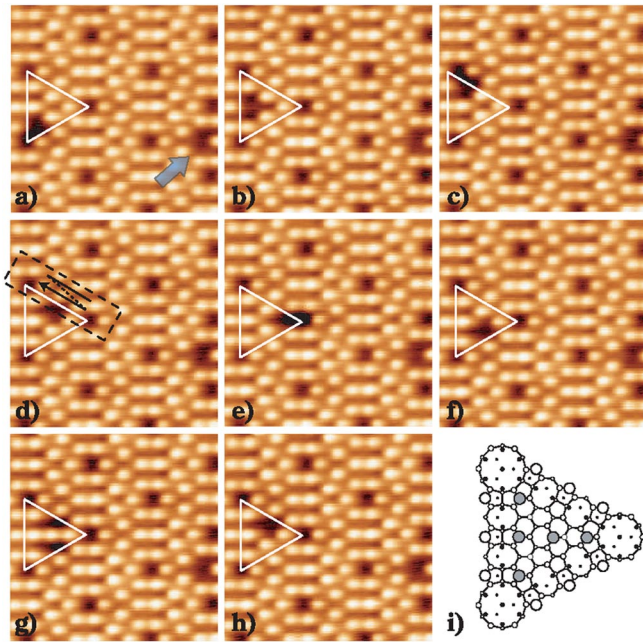
FIG. 1 (color online).   Topographic images, (a) to (h), from a
series of vacancy-mediated manipulations of intrinsic adatoms of
the Si(111)-(7 × 7) surface—a movie is available in EPAPS
[22]. The vacancy pointed out by an arrow in (a) serves as a
marker. First mechanical resonant frequency (f_0), cantilever
oscillation amplitude (A), and cantilever spring constant (K)
were 162295.8 Hz, 282 Å, and 28.7 N/m, respectively.
Imaging (Δf_I) and manipulation (Δf_M) frequency shift set
points were -3.9 and -5.1 Hz, corresponding to an attractive
SR force at closest approach of -0.15 and -0.5 nN [22],
respectively. Image dimensions are (8.0 × 8.0) nm^2. In (i), a
model of the atomic configuration for the highlighted unit cell in
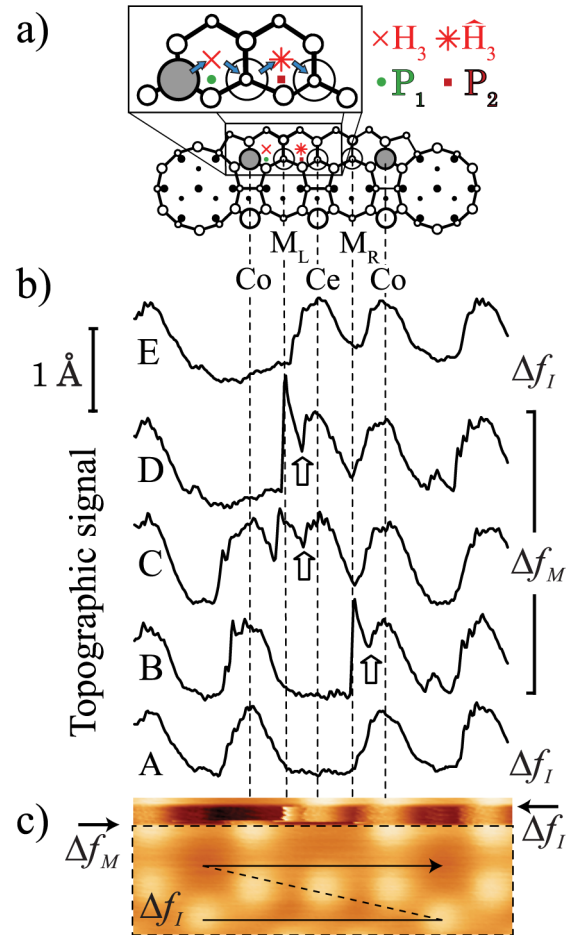(g) is displayed.

FIG. 2 (color online).   (a) Ball-and-stick model of the dimer-
row region of a Si(111)-(7 × 7) faulted half-unit cell with a
vacancy on a center (Ce) adatom site. The corner (Co) adatom
sites, two equivalent M sites (M_L and M_R), and two H$_3$ adsorp-
tion positions together with two tip locations (P_1 and P_2) are
indicated. A detailed view of the Co $\rightarrow$ Ce manipulation path is
shown in the upper part. (b) Line profiles obtained from (c),
where the topography associated with the manipulation process
between the images in Figs. 1(d) and 1(e) is displayed. The
dotted-line rectangle corresponds to the one marked in Fig. 1(d).
The fast scan velocity was 8.6 nm/s, and the rectangle dimen-
sions are (4.3 × 1.5) nm^2.

the arrows that indicate the scan lines at which the set point
was changed to Δf_M and restored to Δf_I, respectively.
Five profiles from this stripe are displayed in Fig. 2(b).
Profiles B to D are sequential, and they correspond with
three different stages of the process: before (B), during (C),
and after (D) the manipulation. In profile A, two adatoms
are seen at corner (Co) sites (left and right) and the vacancy
is at the center (Ce) site. In profile B, once the left corner
adatom and the vacancy have been imaged, the feedback
suddenly retracts the tip at the M_R position due to the jump
of the right corner adatom towards the tip; when still
imaging the adatom (now on the M_R site), at the tip
location marked by the arrow, it jumps back to the right
corner site, where the adatom is imaged again. In profile C,
the tip initially encounters and passes over the adatom on
the left corner site and, between the P_1 and the M_L posi-
tions, it is suddenly retracted due to the jump of the adatom
from the left corner to the M_L site, which subsequently
jumps again to the center site at the tip location marked by
the arrow. Finally, the adatom is imaged at the center site
together with the one at the right corner site that does not
further move. In profile D, just after imaging the vacancy,

the center adatom jumps towards the tip and adsorbs on the
M_L site; it returns to center site afterwards, again at a
position aligned with P_2 and $\hat{H}_3$ (arrow). Further line scans
mimic profile D all over the stripe with jumps at several
locations near M_L until recovering the Δf_I set point. This
is visualized as the bright feature near the M_L position in
Fig. 2(c). In profile E, the vacancy is finally at the left
corner site in contrast with profile A.

The comparison of these profiles with previously re-
ported topographic signatures in STM manipulation ex-
periments performed at cryogenic temperatures [6,15]
indicates that the here reported manipulations can be clas-
sified into the so-called pulling mode [6], in which an
attractive interaction force with the tip-apex pulls the

surface adatom towards the tip position. The high stability shown by the adatoms during imaging (Fig. 1) and the jumps observed in the manipulation profiles [Fig. 2(b)] suggest a mechanism where the tip very locally smooths out the surface energy landscape, enabling the thermally activated hopping [16,17] of the closest adatom to and from adjacent stable adsorption sites, so that the directionality imposed by the tip scan together with the asymmetric potential energy landscape created by the particular tip-apex structure [18,19] during the approaching stage of the successive oscillation cycles produce the adatom manipulation.

These ideas are further substantiated with an extensive study by first-principles simulations of the energetics and stability of the Si(111)-(7 × 7) adatoms in the presence of a vacancy, as well as the modifications induced by the AFM tip. Our calculations are based on FIREBALL, a fast local basis set density functional theory code [20]. We have used a supercell approach (including 347 atoms), where the reconstructed surface is represented by a 7-layer slab with the bottom layer saturated by H atoms, and the AFM tip is modeled with a well-tested [21] Si(111) nanoasperity of ten atoms (inset in Fig. 3) that closely reproduces the experimental SR forces obtained over the Si adatom [22] and fulfills the symmetry expected from the observations during the manipulation experiments [19]. Only the H-saturated last Si layer in both the tip and the slab are kept fixed during the structural minimization process. Computational details (including k sampling and convergence criteria) and methodological approaches (like the determination of tip-surface interaction) are the same as in Ref. [21].

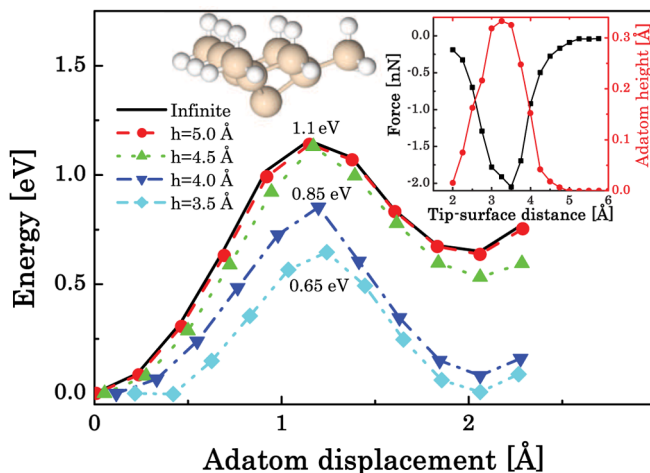In a first stage, we have considered the isolated surface and characterized the potential energy landscape for the

FIG. 3 (color online). Calculated diffusion barriers for the adatom along the $Co \rightarrow H_3$ path when the tip is located at the P_1 position [see Fig. 2(a)] at different tip-surface distances. The two insets show the tip structure (left) and the calculated SR force and related adatom vertical relaxation as a function of the tip-surface distance when the tip is over the P_1 position (right).

diffusion of an adatom close to a vacancy, exploring the energetics even for the vacancy placed at different adatom sites. The energy barriers for the adatom hopping have been estimated using a constrained minimization approach: the adatom is moved in discrete steps along the most energetically favorable trajectory between two adjacent local adsorption minima, letting the system relax to the ground state while keeping the adatom lateral (x, y) coordinates fixed. Based on these calculations, we have identified the path $Co \rightarrow H_3 \rightarrow M_L \rightarrow \hat{H}_3 \rightarrow Ce$ [Fig. 2(a)] as the most energetically favorable for the diffusion of an adatom located on the corner site towards a vacancy at the center site. The large energy barriers found for some of the individual steps (e.g., >1.5 eV for the $M_L \rightarrow H_3$ transition, see Table I) precludes the natural diffusion at RT, in agreement with the experimental observations under imaging conditions (Δf_I set point).

To analyze the influence of the tip, we have recalculated the barriers for several tip-surface distances and different tip lateral positions [including those that the tip follows in the manipulation scan lines, see Fig. 2(a)], allowing the atoms of both the tip and the slab to relax during the energy minimization. Figure 3 illustrates the main modifications in the energy landscape induced by the tip presence, displaying the calculated barriers at several tip-surface distances for the $Co \rightarrow H_3$ transition—one of the more difficult jumps, see Table I—when the tip is located at P_1 [Fig. 2]. As the tip-surface distance is reduced below 5 Å, there is a substantial reduction of the barriers together with an energetic stabilization of the, initially metastable, final adsorption positions—the H_3 site in this case. This behavior can be understood in terms of the tip-surface SR forces and the adatom displacement calculated during the tip approach towards the surface at the position P_1 (inset in Fig. 3). The onset of significant attractive forces below 5 Å—associated with the covalent interaction between the tip and the surface dangling bonds—induces pronounced vertical relaxations on the adatom (Fig. 3), the surrounding surface atoms, and the outermost tip atoms. These relaxations weaken the adatom bonds with the underlying Si atoms, leading to a local reduction of the energy barrier for its in-plane diffusion to an adjacent empty adsorption site along the tip lateral trajectory. The tip presence nearby this originally metastable site further stabilizes the adsorption by offering an extra bond with the tip-apex outermost atom.

These results have important implications for the manipulation. As Fig. 3 shows, for tip-surface distances corresponding to calculated SR forces around the experimental values used during the manipulations (near -0.5 nN, see [22]), the barrier is reduced close to the limit that enables instantaneous thermally activated jumps between the two sites at RT (~ 0.8 eV) [23]. Similar significant reductions on the calculated energy barriers (Table I) are also found for the rest of the transitions between adjacent adsorption sites when the tip is located close to the

TABLE I. Calculated energy barriers (eV) for the transitions between adjacent adsorption sites along the manipulation path with the tip placed close to the relevant lateral positions where adatom displacements [Fig. 2(b)] are observed.

Tip height \ Tip position	P_1 $Co \rightarrow H_3$	M_L $H_3 \rightarrow M_L$	P_2 $M_L \rightarrow \hat{H}_3$	Ce $\hat{H}_3 \rightarrow Ce$
≥ 6 Å	1.16	0.89	1.54	0.64
4 Å	0.86	0.27	0.89	0.16

relevant lateral position along the manipulation path where the adatom's jumps are observed [Figs. 2(a) and 2(b)].

The computational cost precludes a complete, systematic study of the influence of the tip position for all those barriers. Nevertheless, we have performed a quite extensive search for the optimal lateral tip position for the two more difficult steps: $Co \rightarrow H_3$ and $M_L \rightarrow \hat{H}_3$. For both cases, we have found optimal tip positions close to those estimated from the experiments, P_1 and P_2, respectively [Fig. 2(a)]. Our quantification of the tip influence is also limited by the (x, y) adatom path we impose in our constrained minimization approach and the limited elastic response of the tip apex, quite rigid due to the small size of our model tip. However, the consideration of these two effects would lead to a further reduction of the barriers in the presence of the tip, thus confirming our main conclusions regarding the manipulation mechanism.

In summary, we have provided a detailed atomistic description of room-temperature lateral atomic manipulations on a semiconductor surface using dynamic force microscopy. At relevant lateral positions along the manipulation path, the attractive covalent interaction between the semiconductor tip and the surface dangling bonds induces pronounced atomic relaxations on both tip and surface that substantially reduce, very locally, the energy barriers for the adatom hopping to adjacent available adsorption sites—in good agreement with previous experimental results [7,24]—and further stabilizes the adsorption. By gently tuning this interaction, it is relatively easily to reduce these barriers below the limit that enables instantaneous thermally activated hopping at room temperature and use then the directionality imposed by the tip global movement to control the adatom net displacement.

[1] D. M. Eigler and E. K. Schweizer, Nature (London) **344**, 524 (1990).
[2] M. F. Crommie, C. P. Lutz, and D. M. Eigler, Science **262**, 218 (1993).
[3] S.-W. Hla, L. Bartels, G. Meyer, and K.-H. Rieder, Phys. Rev. Lett. **85**, 2777 (2000).
[4] A. J. Heinrich, C. P. Lutz, J. A. Gupta, and D. M. Eigler, Science **298**, 1381 (2002).
[5] G. V. Nazin, X. H. Qiu, and W. Ho, Science **302**, 77 (2003).
[6] L. Bartels, G. Meyer, and K.-H. Rieder, Phys. Rev. Lett. **79**, 697 (1997).
[7] Y. Sugimoto, M. Abe, S. Hirayama, N. Oyabu, O. Custance, and S. Morita, Nat. Mater. **4**, 156 (2005).
[8] I. Horcas *et al.*, Rev. Sci. Instrum. **78**, 013705 (2007).
[9] T. R. Albrecht, P. Grütter, D. Horne, and D. Rugar, J. Appl. Phys. **69**, 668 (1991).
[10] M. Abe, Y. Sugimoto, O. Custance, and S. Morita, Appl. Phys. Lett. **87**, 173503 (2005).
[11] M. Abe, Y. Sugimoto, O. Custance, and S. Morita, Nanotechnology **16**, 3029 (2005).
[12] N. Oyabu, O. Custance, I. Yi, Y. Sugawara, and S. Morita, Phys. Rev. Lett. **90**, 176102 (2003).
[13] Faulted and unfaulted half-unit cells were assigned by standard STM measurements, keeping the relative tip-sample orientation afterwards.
[14] S. Kawai and H. Kawakatsu, Appl. Phys. Lett. **89**, 023113 (2006).
[15] S.-W. Hla, K.-F. Braun, and K.-H. Rieder, Phys. Rev. B **67**, 201402(R) (2003).
[16] G. Meyer, L. Bartels, S. Zöphel, E. Henze, and K.-H. Rieder, Phys. Rev. Lett. **78**, 1512 (1997).
[17] M. B. Watkins and A. L. Shluger, Phys. Rev. B **73**, 245435 (2006).
[18] L. Pizzagalli and A. Baratoff, Phys. Rev. B **68**, 115427 (2003).
[19] Lateral manipulations depend strongly on the tip-apex structure and, thus, different Δf_M set points are normally required for each surface crystallographic direction [7,18]. In the series shown in Fig. 1, however, the same Δf_M set point was used for all the manipulations, pointing towards a highly symmetric tip apex.
[20] P. Jelinek, H. Wang, J. P. Lewis, O. F. Sankey, and J. Ortega, Phys. Rev. B **71**, 235101 (2005).
[21] N. Oyabu, P. Pou, Y. Sugimoto, P. Jelinek, M. Abe, S. Morita, R. Pérez, and O. Custance, Phys. Rev. Lett. **96**, 106101 (2006).
[22] See EPAPS Document No. E-PRLTAO-98-078710 for additional information. For more information on EPAPS, see http://www.aip.org/pubservs/epaps.html.
[23] I. Brihuega, O. Custance, and J. M. Gómez-Rodríguez, Phys. Rev. B **70**, 165410 (2004).
[24] N. Oyabu, Y. Sugimoto, M. Abe, O. Custance, and S. Morita, Nanotechnology **16**, S112 (2005).